Damage Classification Structural Health Monitoring in Bolted Structures Using Time-frequency Techniques

DEBEJYO CHAKRABORTY[1], NARAYAN KOVVALI,[1,*] JUN WEI[2], ANTONIA PAPANDREOU-SUPPAPPOLA[1]
DOUGLAS COCHRAN[1] AND ADITI CHATTOPADHYAY[2]

[1]*Department of Electrical Engineering, Arizona State University, Tempe, AZ, USA*

[2]*Department of Mechanical and Aerospace Engineering, Arizona State University, Tempe, AZ, USA*

ABSTRACT: The analysis, detection, and classification of damage in complex bolted structures is an important component of structural health monitoring. In this article, an advanced signal processing and classification method is introduced based on time-frequency techniques. The time-varying signals collected from sensors are decomposed into linear combinations of highly localized Gaussian functions using the matching pursuit decomposition algorithm. These functions are chosen from a dictionary of time-frequency shifted and scaled versions of an elementary Gaussian basis function. The dictionary is also modified to use real measured data as the basis elements in order to obtain a more parsimonious signal representation. Classification is then achieved by matching the extracted damage features in the time-frequency plane. To further improve classification performance, the information collected from multiple sensors is integrated using a Bayesian sensor fusion approach. Results are presented demonstrating the algorithm performance for classifying signals obtained from various types of fastener failure damage in an aluminum plate.

Key Words: Structural health monitoring, damage classification, time-frequency analysis, matching pursuit decomposition, sensor fusion, fastener failure.

INTRODUCTION

STRUCTURAL health monitoring (SHM) (Staszewski et al., 2004; Farrar and Worden, 2007) is a problem of interest in many applications, including civil, mechanical, and aerospace engineering. It involves *in situ* sensing and analysis of structural characteristics to detect changes in features that may indicate the presence of damage or degradation. The presence of damage can adversely affect the current or future performance of the system (Farrar and Worden, 2007). The goal of SHM is to identify, locate, and quantify damage for state-awareness of key structural components.

A considerable amount of literature, in the fields of mechanical, material, and structural engineering, and signal processing and statistical analysis (Staszewski et al., 2004; Farrar and Lieven, 2007; Farrar and Worden, 2007), exists on methodologies for determining the presence, type, location, and intensity of structural damage. Some examples include statistical methods (Doebling and Farrar, 1998; Farrar et al., 1999), time-series analysis (Sohn and Farrar, 2001), statistical pattern recognition (Sohn et al., 2001), impedance-based methods (Park et al., 2003), Fourier component pair analysis (Gelman et al., 2004), Bayesian methods (Sohn and Law, 2000; Nguyen et al., 2004), extreme value statistics (Sohn et al., 2005), and support vector machines (Das et al., 2007). Mechanical, material, and structural methods can provide physically based damage models to describe the propagation of waves through materials. On the other hand, signal processing and statistical analysis algorithms can provide effective representations to extract the information-content of collected data, leading to efficient and reliable systems for damage inference.

In this article, a novel damage analysis and classification technique is presented, which is based on the use of time-frequency analysis (Hlawatsch and Boudreaux-Bartels, 1992; Cohen, 1994; Papandreou-Suppappola, 2002). As the propagation of waves in materials can be characterized as a dispersive or time-varying phenomenon, due to structures behaving as wave-guides, the measured vibration data has spectral information that varies with time. This time-varying signal signature cannot be adequately characterized using standard time-domain or frequency-domain techniques. The natural tool to use is a joint time-frequency approach that is effective in capturing the dynamics of the physical

*Author to whom correspondence should be addressed.
E-mail: narayan.kovvali@asu.edu
Figures 2, 3, 6–9 and 11–13 appear in color online: http://jim.sagepub.com

1045-389X/09/11 1289–17 $10.00/0 DOI: 10.1177/1045389X08100044

process and results in an informative framework for structural and material damage identification. Time-frequency techniques are, therefore, utilized to analyze structural data as indicators of damage.

Various time-frequency methods have been considered for damage detection and classification, including the instantaneous frequency (Bernal and Gunes, 2000) and the spectrogram time-frequency representation (TFR) (Altes, 1980, Vincent et al., 1994; Karasaridis et al., 1997). If high resolution is important, the Wigner distribution (WD) TFR (Hlawatsch and Boudreaux-Bartels, 1992; Cohen, 1994) is often chosen as the spectrogram has limited time and frequency resolution properties. The WD, on the other hand, exhibits cross-terms when the signals are multi-component, and the presence of cross-terms could yield incorrect information if not properly processed. The wavelet transform (Mallat, 1998) is a time-scale representation that has been used extensively for damage detection (Jeong and Jang, 2000; Paget, et al., 2003; Eren and Devaney, 2004; Sun and Chang, 2004; Taha et al., 2006; Pakrashia et al., 2007). However, the wavelet transform can result in low resolution in time or frequency, depending on the value of the frequency. Although wavelet packets can be used to mitigate this issue to a certain extent, the representation remains non-adaptive to signal changes (Mallat, 1998).

The matching pursuit decomposition (MPD) method (Mallat and Zhang, 1993; Mallat, 1998) is chosen in this paper as it is a time-frequency signal representation technique that does not have the aforementioned limitations. The MPD can be used to obtain a new TFR (MPT-TFR) that can adapt to the signal structure. This is because the MPD decomposes a signal into highly-localized Gaussian atoms in the time-frequency plane. It is thus well-matched to the signals being analyzed, yielding parsimonious representations. By appropriately designing the MPD dictionary, the MPD-TFR can be free of cross-terms and can also yield high resolution in both time and frequency. Due to its iterative nature, the algorithm can also be used to reduce measurement noise, and if a Gaussian dictionary is used, this can be achieved with only a modest increase in computational effort (Mallat and Zhang, 1993).

The MPD algorithm is based on extracting signal time-frequency features from a dictionary of basis atoms. In this article, two different types of basis atoms are considered: time-shifted, frequency-shifted, and scaled Gaussian signals and time-frequency shifted real data matched to the analysis data. The Gaussian dictionary results in a highly localized MPD representation as the Gaussian signals are the most concentrated signals in both time and frequency simultaneously (Mallat and Zhang, 1993). The data-matched dictionary results in a highly parsimonious representation that can be more efficiently computed (Papandreou-Suppappola and Suppappola 2002). The MPD-TFRs are thus useful in extracting characteristic time-frequency features from the measured signals, and they have been used for analysis, detection, and classification (Ebenezer et al., 2004; Das et al., 2005).

Classification of damage can be performed by matching the extracted damage features in the time-frequency plane. Specifically, for the MPD-TFR-based damage classifier, representative template TFRs of training data are used to characterize the time-frequency structure of each damage state yielding different damage classes. A test data is then classified based on the strength of the correlation of its MPD-TFR with the template TFRs in the time-frequency plane. In order to increase analysis and classification performance, it is common to collect structural data from multiple distributed sensors. Here, a Bayesian sensor decision fusion approach is used to combine the information gathered by all the sensors. Classification is first performed independently using data from each sensor, and local decisions are then optimally combined in a Bayesian decision fusion center to obtain a global decision.

The remainder of this paper is organized as follows. In section 'Matching Pursuit Decomposition', the MPD algorithm is described in detail, and the corresponding MPD classifier is provided in section 'MPD Classifier for Damage Classification' for different MPD dictionaries. section 'Classification of Structural Data' demonstrates the classification performance of the proposed technique by considering fastener failure damage in an aluminum plate. In section 'Bayesian Sensor Fusion', the Bayesian decision fusion approach is described to order to integrate the information gathered from multiple sensors, and results are shown to demonstrate the increased classification performance. The Appendix provides the finite element analysis used to optimize the MPD classifier performance.

MATCHING PURSUIT DECOMPOSITION

MPD Algorithm

The MPD algorithm (Mallat and Zhang, 1993; Mallat, 1998) is an iterative processing method that expands a signal into a weighted linear combination of elementary basis functions or "atoms" chosen from a complete dictionary. The resulting expansion of a finite energy signal $x(t)$ is given by

$$x(t) = \sum_{i=0}^{\infty} \alpha_i g_i(t),$$

where $g_i(t)$ is the basis function selected from the MPD dictionary $\mathcal{D}$ at the ith MPD iteration and α_i is the corresponding expansion coefficient. The expansion is such that the energy E_x of the signal is preserved. In particular, if the basis functions $g_i(t)$ are normalized to unit energy, then it can be shown that

$$E_x = (\|x\|_2)^2 \triangleq \int_{-\infty}^{\infty} x(t)x^*(t)\mathrm{d}t = \sum_{i=0}^{\infty} |\alpha_i|^2.$$

After N iterations, the resulting expansion can be shown to converge in the L_2 sense, i.e.,

$$\lim_{N\to\infty} \|x(t) - \sum_{i=0}^{N-1} \alpha_i g_i(t)\|_2 = 0.$$

In practical applications, the MPD signal expansion is thus given by

$$x(t) = \sum_{i=0}^{N-1} \alpha_i g_i(t) + r_N(t), \tag{2.1}$$

where $r_N(t)$ is the residual signal after N MPD iterations such that

$$(\|x\|_2)^2 = \left(\sum_{i=0}^{N-1} |\alpha_i|^2\right) + (\|r_N\|_2)^2.$$

The steps of the MPD iterative algorithm are given as follows (Mallat and Zhang, 1993, Mallat, 1998). With $r_0(t) = x(t)$, at the ith iteration, $i = 0, 1, \ldots, N-1$, the projection of the residue $r_i(t)$ onto every dictionary element $g^{(d)}(t) \in \mathcal{D}$ is computed to obtain

$$\Lambda_i^{(d)} = \left\langle r_i, g^{(d)} \right\rangle \triangleq \int_{-\infty}^{\infty} r_i(t) g^{(d)} * (t)\mathrm{d}t.$$

The selected dictionary atom $g_i(t)$ is the one that maximizes the magnitude of the projection,

$$g_i(t) = \underset{g^{(d)}(t)\in\mathcal{D}}{\operatorname{argmax}} \left|\Lambda_i^{(d)}\right|. \tag{2.2}$$

The corresponding expansion coefficient is

$$\alpha_i = \langle r_i, g_i \rangle = \int_{-\infty}^{\infty} r_i(t) g_i(t)\mathrm{d}t. \tag{2.3}$$

The residues at the ith and $(i+1)$th iterations are related as $r_{i+1}(t) = r_i(t) - \alpha_i g_i(t)$. Thus, after N MPD iterations, the residue is given by

$$r_N(t) = r_{N-1}(t) - \alpha_{N-1} g_{N-1}(t) = x(t) - \sum_{i=0}^{N-1} \alpha_i g_i(t).$$

It can be shown that the residue energy progressively decreases as the number of iterations increases, i.e., $(\|x\|_2)^2 = (\|r_0\|_2)^2 \geq (\|r_1\|_2)^2 \geq \cdots \geq (\|r_N\|_2)^2 \geq 0$.

The truncation limit N is usually chosen such that the energy of the residue after N iterations is smaller than some pre-defined value. Note that, by design, the MPD yields a compact representation of a signal in terms of selected basis functions in the dictionary. In addition, it effectively filters out unwanted signal components such as noise because the noise subspace is typically orthogonal to that spanned by the dictionary elements (Mallat and Zhang, 1993). The MPD algorithm is summarized in the flowchart in Figure 1.

The MPD dictionary consists of a redundant set of atoms which, in general, do not have to form an orthonormal set; the dictionary is, however, required to be complete (Mallat and Zhang, 1993). The dictionary is formed by time-frequency shifting and scaling a basic atom. In (Mallat and Zhang, 1993), the basic atom is chosen to be a Gaussian signal, given by $g(t) = (2/\pi)^{1/4} e^{-t^2}$. This basic atom has unit energy and

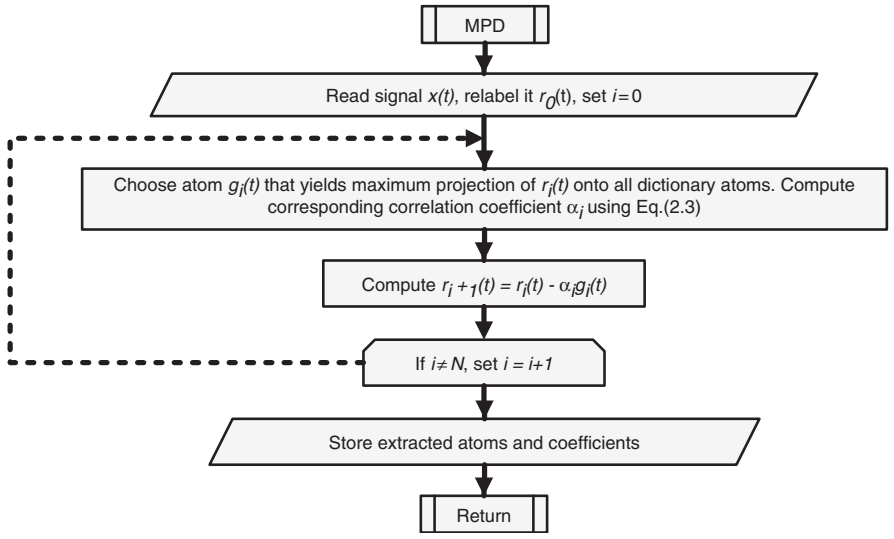

Figure 1. *MPD algorithm.*

is concentrated at the origin $(t,f) = (0,0)$ in the time-frequency plane. The shifting transformations result in moving the atom in the time-frequency plane, and the scaling transformation changes the variance (or spread in time) of the Gaussian function. Specifically, the transformed basis functions that form the dictionary $\mathcal{D}$ are given by

$$g^{(d)}(t) = (2\kappa_l/\pi)^{1/4} e^{-\kappa_l(t-\tau_n)^2} e^{j2\pi\nu_m t}, \tag{2.4}$$

where $d = \{\tau_n, \nu_m, \kappa_l\}$ is the set of all time-shifted (by $\tau_n, n = 1, \ldots, N_d$), frequency-shifted (by $\nu_m, m = 1, \ldots, M_d$), and time-scaled (by $\kappa_l > 0, l = 1, \ldots, L_d$) atoms that are normalized to have unit energy. If $x(t)$ is real, then the dictionary can be formed using real unit energy Gaussian atoms, given by $g^{(d)}(t) = (8\kappa_l/\pi)^{1/4} e^{-\kappa_l(t-\tau_n)^2} \cos(2\pi\nu_m t)$.

The computational complexity of the MPD algorithm is $O(N_x \log N_x)$ (Mallat and Zhang, 1993), where N_x is the number of available samples of the signal $x(t)$. This computational cost is the result of a few facts. First, each projection of the residue signal onto the time-shifted atoms at every MPD iteration can be interpreted as a correlation that can be efficiently implemented using the fast Fourier transform (FFT) with $O(N_x \log N_x)$ computational complexity. In addition, the cost of the FFT of the Gaussian atoms, needed to obtain the frequency shift in (2.4), can be reduced by analytically computing the transforms. Specifically, the Fourier transform of a frequency-shifted Gaussian atom $e^{-\kappa t^2} e^{j2\pi\nu t}$ is a Gaussian function in the frequency domain given by $\sqrt{\pi/\kappa} e^{\left(-(f-\nu)^2/(4\kappa)\right)}$. The computational cost can be further reduced by storing the frequency shifts of the Gaussian atoms ahead of time to use only when needed .

MPD-based TFR

The choice of dictionary basis functions used in the MPD algorithm depends on the application. In the present problem, the analysis signals propagate through dispersive media, and as a result, they exhibit time-varying spectral characteristics as their frequency content can change with time. Thus, they are best analyzed using time-frequency techniques that are designed to depict time-varying spectra in the time-frequency plane (Hlawatsch and Boudreaux-Bartels, 1992; Cohen, 1994; Papandreou-Suppappola, 2002). The WD is a popular TFR as it does not exhibit windowing effects when analyzing signals, thus providing high time-frequency resolution properties. For a signal $x(t)$, the WD is defined as

$$\mathrm{WD}_x(t,f) \equiv \int_{-\infty}^{\infty} x\left(t + \frac{\tau}{2}\right) x^*\left(t - \frac{\tau}{2}\right) e^{-j2\pi f\tau} \mathrm{d}\tau.$$

The WD is well-matched to the MPD framework as the WD preserves time-frequency shifts and scale changes as in (2.4). Specifically, the WD satisfies the following three properties:

$$y(t) = x(t-\tau) \Rightarrow \mathrm{WD}_y(t,f) = \mathrm{WD}_x(t-\tau, f)$$
$$y(t) = x(t)e^{j2\pi\nu t} \Rightarrow \mathrm{WD}_y(t,f) = \mathrm{WD}_x(t, f-\nu)$$
$$y(t) = \sqrt{|\kappa|}x(\kappa t) \Rightarrow \mathrm{WD}_y(t,f) = \mathrm{WD}_x(\kappa t, f/\kappa).$$

Using these properties, the WD of the Gaussian function $g(t)$ is related to the WD of the transformed Gaussian atom $g^{(d)}(t)$ as $\mathrm{WD}_{g^{(d)}}(t,f) = \mathrm{WD}_g(\kappa_l(t-\tau_n), (f-\nu_m)/\kappa_l)$. Also, the WD of the Gaussian atoms $g^{(d)}(t)$ in (2.4) can be computed analytically (Mallat and Zhang, 1993) as

$$\mathrm{WD}_{g^{(d)}}(t,f) = (1/(2\pi\kappa_l)) e^{-2\pi\kappa_l(t-\tau_n)^2} e^{-2\pi(f-\nu_m)^2/\kappa_l}. \tag{2.5}$$

As Gaussian signals are the most concentrated signals in both time and frequency according to the uncertainty principle (Hlawatsch and Boudreaux-Bartels, 1992), their WD is highly localized, in addition to being easy to compute using the closed-form expression in (2.5).

The main drawback of the WD TFR is the presence of cross terms when used to analyze signals with multiple time-frequency components due to its quadratic nature. Essentially, if a signal consists of multiple components, the WD of the signal is not only the sum of the WDs of the components, but also the cross WD between any two components (Hlawatsch and Boudreaux-Bartels, 1992). In order to avoid cross-terms, the MPD-TFR is defined as the sum of the weighted WDs of each of the selected atoms (Mallat and Zhang, 1993)

$$\mathscr{E}_x(t,f) \equiv \sum_{i=0}^{N-1} |\alpha_i|^2 \mathrm{WD}_{g_i}(t,f). \tag{2.6}$$

Since $\mathrm{WD}_{g_i}(t,f)$ is the WD of the selected atom $g_i(t)$ in the ith MPD iteration, and this atom consists of a single Gaussian, the MPD-TFR in (2.6) is free of cross-terms. An example of the sum of the WD of $N = 4$ time-frequency transformed Gaussian atoms is shown in Figure 2. The corresponding time-frequency shifts and scale changes of the four atoms are marked on the time-frequency plot in Figure 2.

Demonstration of the MPD Algorithm and MPD-TFR

The use of the MPD algorithm in decomposing a signal and the corresponding MPD-TFR of the signal is demonstrated with a simple example. A simulated signal

is considered that consists of the sum of two Gaussian functions

$$x(t) = e^{-40{,}000(t-0.025)^2} e^{j2\pi 1000t} + e^{-40{,}000(t-0.025)^2} e^{j2\pi 2000t}. \tag{2.7}$$

The first Gaussian function is time-shifted by $\tau = 25$ ms, frequency-shifted by $\nu = 1$ kHz, and scaled by $\kappa = 40000$. The second Gaussian function is time-shifted and scaled by the same amounts as the first Gaussian, but frequency-shifted by $\nu = 2$ kHz. Figure 3 shows the WD of $x(t)$, where the cross term between the two auto WDs (corresponding to the WD of each single Gaussian component) can be seen halfway between the two auto terms at $(t,f) = (25$ ms, 1.5 kHz). When the signal in (2.7) is decomposed using the MPD, as the MPD dictionary does contain these two Gaussian atoms, the algorithm converges after only $N = 2$ iterations. The extracted atoms correspond to exactly the two signal components and the residue is identically zero. Note that, in general, this will not be true for most real signals; it was designed to be so here, in order to emphasize the high time-frequency localization and no-cross-term properties of the MPD-TFR. The resulting MPD-TFR in (2.6) is shown in Figure 3 without any cross-terms.

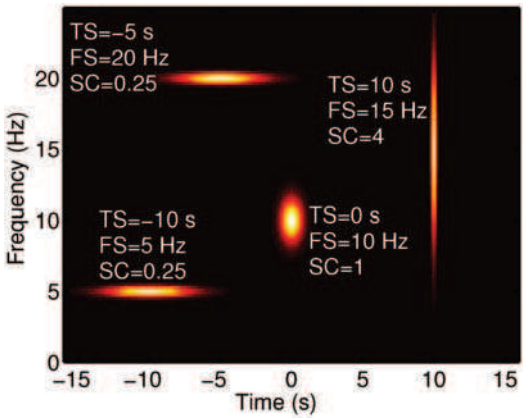

Figure 2. *Sum of the WDs of $N = 4$ time-frequency shifted and scaled Gaussian atoms from an MPD dictionary. Here, TS denotes time shift, FS is frequency shift and SC is scale change.*

MPD CLASSIFIER FOR DAMAGE CLASSIFICATION

Classification Using MPD

The SHM problem of analyzing and classifying measured signals from structures at different levels of damage conditions (referred to as damage classes) is considered. As the MPD algorithm decomposes a signal into highly localized basis functions, the MPD-TFR can be used for damage classification by exploiting the time-frequency features extracted by the MPD (Papandreou-Suppappola and Suppappola, 2002; Ebenezer et al., 2004). There are two main steps in this classification algorithm. The first step is to train the MPD classifier using a representative set of training signals from damaged classes of interest. The second step is to classify the MPD extracted features of a test signal using the MPD extracted features of the training signals in the time-frequency plane.

Specifically, the MPDs of training signals from different damage classes are first computed, and the corresponding MPD-TFRs of the training signals are used to construct template TFRs that represent the time-frequency characteristics of each damage class. Given M classes corresponding to signals from M different types of damages, a training signal for class m, $m = 1, \ldots, M$, is denoted as $y_{l,m}(t)$, where $l = 1, \ldots, L_m$ and L_m is the number of training signals used for class m. The MPD-TFR for each training signal is computed as

$$\mathscr{E}_{y_l,m}(t,f) = \sum_{i=0}^{N-1} |\alpha_i, m, l|^2 \mathrm{W}D_{g_i,m,l}(t,f), \tag{3.1}$$

where $g_{i,m,l}(t)$ and $\alpha_{i,m,l}$ are the selected Gaussian atom and expansion coefficient in the ith MPD iteration for the lth training signal in the mth class. The template TFRs for each class are then computed by averaging the MPD-TFRs of all the training signals in that class as

$$\mathscr{E}_{y_m}(t,f) = \frac{1}{L_m} \sum_{l=1}^{L_m} \mathscr{E}_{y_l,m}(t,f). \tag{3.2}$$

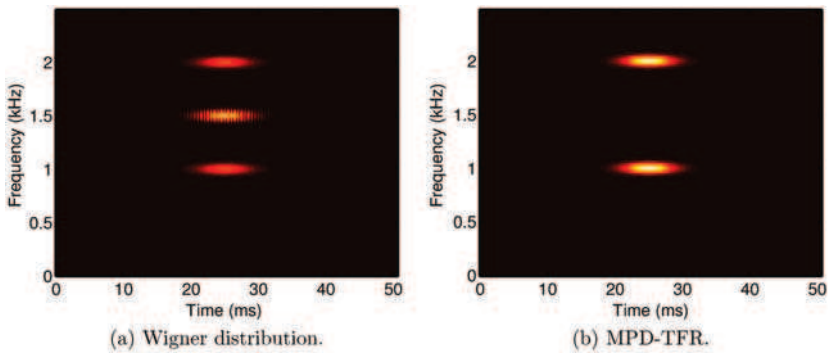

Figure 3. *Comparison of the Wigner distribution and the MPD-TFR of the signal in (2.7).*

Classification is performed using (2D) correlations between template TFRs and the MPD-TFR of the test signal. The strength of the correlations in the time-frequency plane is used to quantify how similar or dissimilar the given signal is to known members of each class. Specifically, given a test signal $x(t)$, its MPD-TFR, $\mathscr{E}_x(t,f)$, is first obtained. Then, $x(t)$ is assigned to Class m^* if

$$m^* = \underset{m=1,\ldots,M}{\operatorname{argmax}} \left\{ \int_{-\infty}^{\infty} \int_{-\infty}^{\infty} \mathscr{E}_x(t,f) \mathscr{E}^*_{ym}(t,f) \mathrm{d}t\, \mathrm{d}f \right\}. \quad (3.3)$$

Note that the MPD-TFRs are normalized to unit L_1-norm before computing the correlations (equivalent to an L_2 signal normalization (Mallat and Zhang, 1993)). The flowchart in Figure 4 summarizes the MPD classification technique.

Note that the larger the number of measurements available for training, the more statistically accurate are the template TFRs, and consequently, the more robust the classifier. In practice, as many training signals should be obtained as possible. Also, in addition to training on multiple signals from the same experiment, it is also desirable to train on measurements from different experiments for the same type of damage and boundary conditions in order to make the classifier more robust. The computational complexity of the MPD classifier can be reduced by writing the relevant MPD-TFRs in terms of their component WDs, and then using the fact that the 2-D Gaussian functions (corresponding to the WDs of each selected Gaussian atom) are uncorrelated in time and frequency (2.5). The 2D integrals in (3.3) can, therefore, be factored into 1D time and frequency integrals of Gaussian functions, which can be computed efficiently.

Modified MPD Classifier

In the MPD damage classification algorithm discussed in Section 'Classification Using MPD' , the

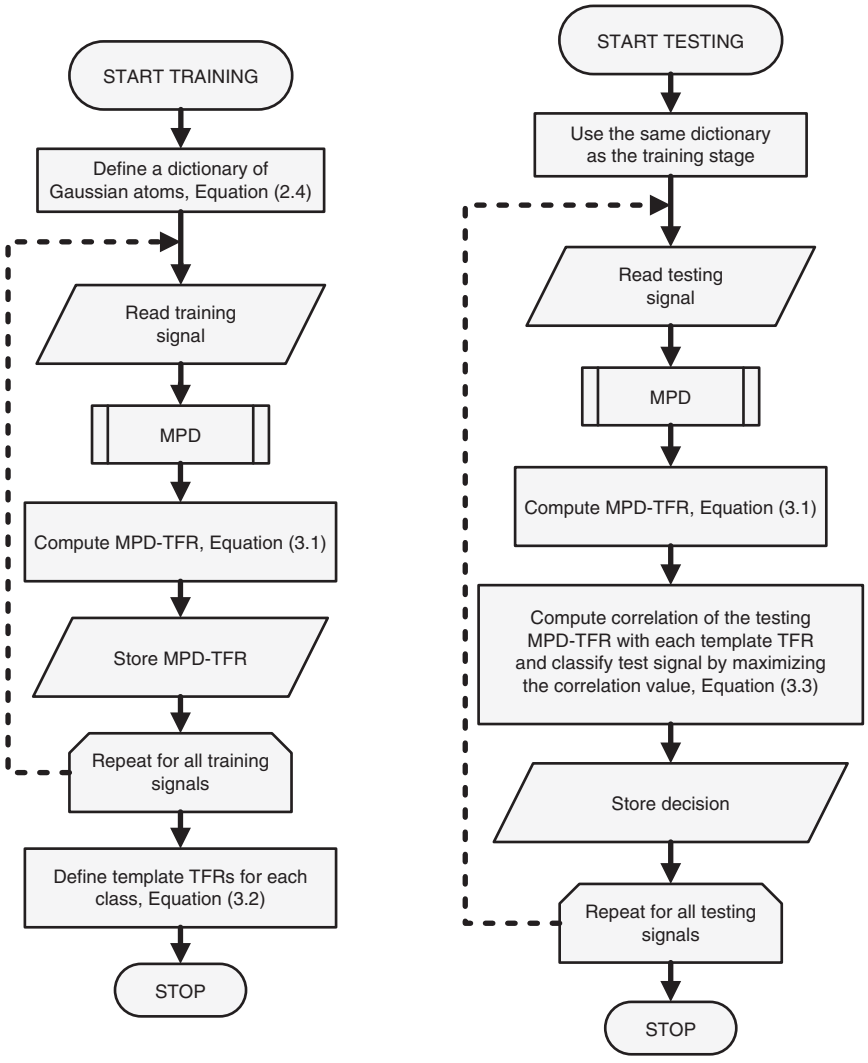

Figure 4. *MPD classification technique.*

dictionary is composed of time-frequency shifted and scaled versions of an elementary Gaussian atom. Since the WD of a Gaussian signal is known in closed-form (2.5), the use of this dictionary can reduce the MPD computational cost. If a signal, however, is not sparse in the time-frequency plane, then a very large number of Gaussian functions will be required in order to accurately represent it.

In the modified MPD (MMPD) algorithm (Papandreou-Suppappola and Suppappola, 2002), the dictionary is composed of time-frequency shifted signals from real sensor measurements. The MMPD-based damage classifier uses the MPD with sensor data obtained directly from structural damage experiments as the dictionary atoms (Ebenezer et al., 2004). As this dictionary is matched specifically to the signals of interest in an application, it has the advantage of yielding highly parsimonious representations.

The MMPD is performed using the MPD steps described in section 'MPD Algorithm' but with the dictionary atoms composed of multiple real signals from each of the M damage classes, with each signal time and frequency shifted to cover the entire time-frequency plane. The dictionary atoms are now denoted as $g_m^{(d)}(t)$, $m = 1, \ldots, M$, to emphasize that time-frequency shifted versions of representative signals from each class need to be included in the dictionary. At the ith MPD iteration, $i = 0, 1, \ldots, N-1$, for a signal $x(t)$, the projection of the residue $r_i(t)$ (with $r_0(t) = x(t)$) onto each dictionary element is computed as

$$\Lambda_{m,i}^{(d)} = \left\langle r_i, g_m^{(d)} \right\rangle.$$

The atom that maximizes the projection is denoted as

$$g_{m,i}(t) = \underset{g_m^{(d)}(t) \in \mathcal{D}}{\operatorname{argmax}} \left\{ |\Lambda_{m,i}^{(d)}| \right\},$$

and is known to belong to class m with corresponding expansion coefficient $\alpha_{m,i}$. The decomposed signal can be approximated as

$$x(t) \approx \sum_{i=0}^{N-1} \alpha_{u,i} g_{u,i}(t), \tag{3.4}$$

where $u \in \{1, \ldots, M\}$ could be any one of the M possible classes.

With the MMPD, the MPD-TFR is not adequate for classification. This is because the WD of an extracted atom could suffer from inner interference terms as the atom (corresponding to a real signal) may have nonlinear time-frequency characteristics (Papandreou-Suppappola, 2002). In this framework, the classification of a given test signal $x(t)$ is not performed in the time-frequency plane. Instead, the magnitude of the projection of the signal onto each damage class becomes the class deciding factor. The projection $\rho_x^{(m)}$ of the signal $x(t)$ onto the mth damage class, $m = 1, \ldots, M$, is computed as

$$\begin{aligned} \rho_x^{(m)} &= \sum_{l=1}^{L_m} \left[\left\langle \sum_{i=0}^{N-1} \alpha_{u,i} g_{u,i}, g_{m,l}^{(d)} \right\rangle \right] = \sum_{l=1}^{L_m} \left[\sum_{i=0}^{N-1} \left\langle \alpha_{u,i} g_{u,i}, g_{m,l}^{(d)} \right\rangle \right] \\ &= \sum_{l=1}^{L_m} \left[\sum_{i=0}^{N-1} \alpha_{u,i} \left\langle g_{u,i}, g_{m,l}^{(d)} \right\rangle \right], \end{aligned} \tag{3.5}$$

where $u \in \{1, 2, \ldots, M\}$ from the decomposition of $x(t)$ in (3.4) and $g_{m,l}^{(d)}(t)$ is the dictionary atom corresponding to the time-frequency shifted version of the lth training signal in the mth class. Furthermore, it can be shown that

$$\left\langle g_u, i, g_{m,l}^{(d)} \right\rangle = \begin{cases} \alpha_{m,i}, & u = m \\ \beta_{m,i}, & u \neq m, \end{cases} \tag{3.6}$$

where $\beta_{m,i}$ is any number that is less than $\alpha_{m,i}$. Equation (3.6) follows from the fact that signals within a class tend to be more correlated. In order to save computation, $\beta_{m,i}$ in (3.6) can be set to zero. Thus, using this result, (3.5) simplifies to

$$\rho_x^{(m)} = \sum_{i=0}^{N-1} |\alpha_u, i|^2 \delta[u - m], \tag{3.7}$$

where $\delta[u - m] = 1$ if $u = m$ and 0 if $u \neq m$.

The resulting classifier assigns test signal $x(t)$ to class m^* if

$$m^* = \underset{m=1,\ldots,M}{\operatorname{argmax}} \left\{ \rho_x^{(m)} \right\}. \tag{3.8}$$

The MMPD-based classification scheme is summarized in the flowchart in Figure 5.

CLASSIFICATION OF STRUCTURAL DATA

Experimental Setup and Data Collection

The type of damage addressed in this article is fastener failure in a square aluminum plate. The experiments for data collection were conducted at the Advanced Structural Concepts Branch, Air force Research Laboratory. The test article is a 12 in. by 12 in. by 0.204 in. aluminum plate (Olson et al., 2006), fastened at the corners with four bolts as shown by the schematic plot in Figure 6. There are four surface mounted piezoelectric transducers (PZTs) of 0.25 in. diameter. PZT1 in Figure 6 is the actuator; PZT2, PZT3, and PZT4 are used as receivers. The orientation is symmetric. Any change in the structural condition (damage) reflects upon the vibrational response of the plate and is encoded by the sensor responses.

The excitation signal used in this experiment was a 0–1.5 kHz linear frequency-modulated (LFM) chirp that induced normal structural vibrations. The MPD- and MMPD-based classifiers are not restricted to this type of excitation (Channels et al., 2008; Chakraborty et al., 2008). Broadband excitation was not used because of experimental and computational difficulties. Specifically, the PZT sensors used had a narrowband response, and high-sampling rates and large dictionaries would be needed in the MPD to accommodate broadband signals. Five different classes of structural damage are defined. Classes 1–4 of damage correspond to bolts 1–4 at 25% torque (30 inch-pound), respectively, and Class 5 (the undamaged class) has all the bolts at 100% torque (120 inch-pound). Responses were collected from the PZTs from multiple measurements, and 400 signals were collected from each PZT and for each damage class. Class 5 had 1600 signals collected at each PZT. A total of 9600 signals were used for classification from all three PZT sensors. The sampling frequency at the transmitter and receiver was 5 kHz. Figure 7 shows example time-domain plots of the signal transmitted by PZT1 and the signals received by PZT3 for the five classes.

Data Preprocessing and MPD

Preprocessing of the received signals and feature extraction helps obtain better classification results. In some cases, however, some loss of useful information is unavoidable. The measured signals were filtered using a (unit-energy) lowpass Butterworth filter that was shifted to the signal mean value to remove the 0 Hz component. This ensures that all the signals have the same energy for correct damage classification.

The MPD was performed with $N = 60$ iterations using a dictionary of real unit-energy Gaussian atoms that are time-shifted, frequency-shifted, and scaled versions of an elementary Gaussian atom. This choice of N corresponds to a residue energy of <10% of the original signal energy. Note that it is not necessary to use the same value of N for all signals. However, N was fixed in order for each signal to have in an equal number of feature vectors (corresponding to expansion coefficients, time-frequency shift values and scale change values).

Using time shifts of 2 s duration and frequency shifts of 1.5 kHz bandwidth, the dictionary consisted of about 42 million atoms. Figure 8 shows an example time-domain Class 1 signal (from PZT3) after its decomposition using

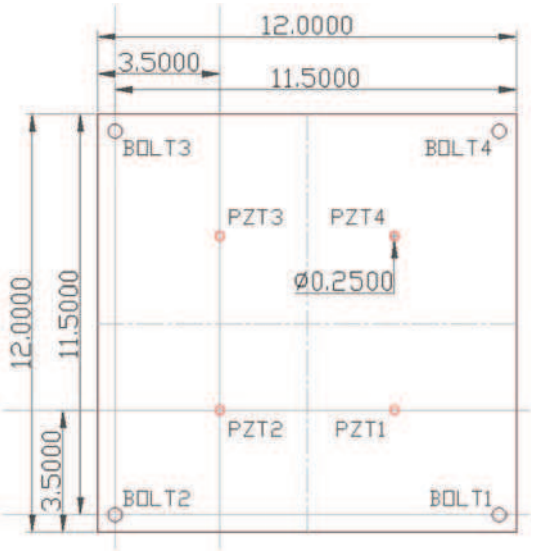

Figure 6. *Experimental setup for fastener damage in a square aluminum plate (Olson et al., 2006) (all dimensions are in inches).*

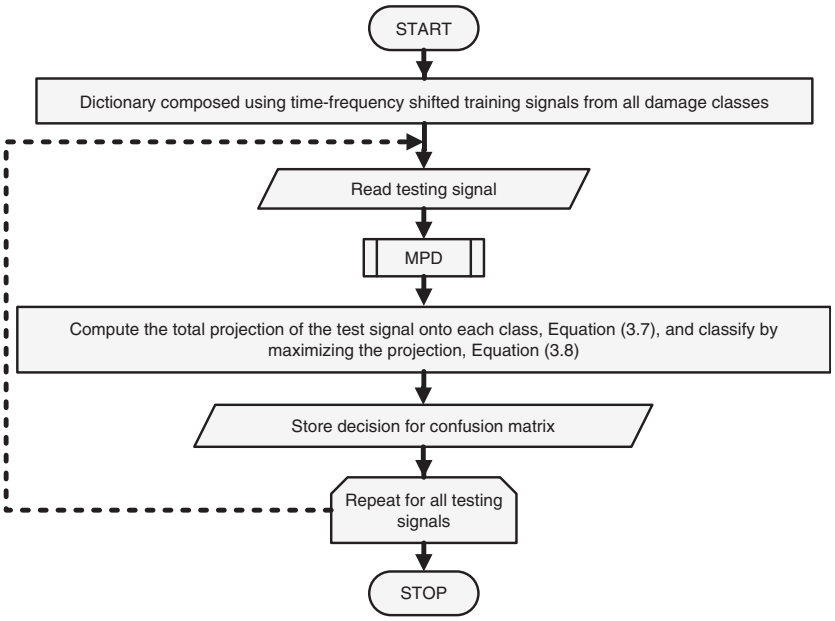

Figure 5. *MMPD classifier.*

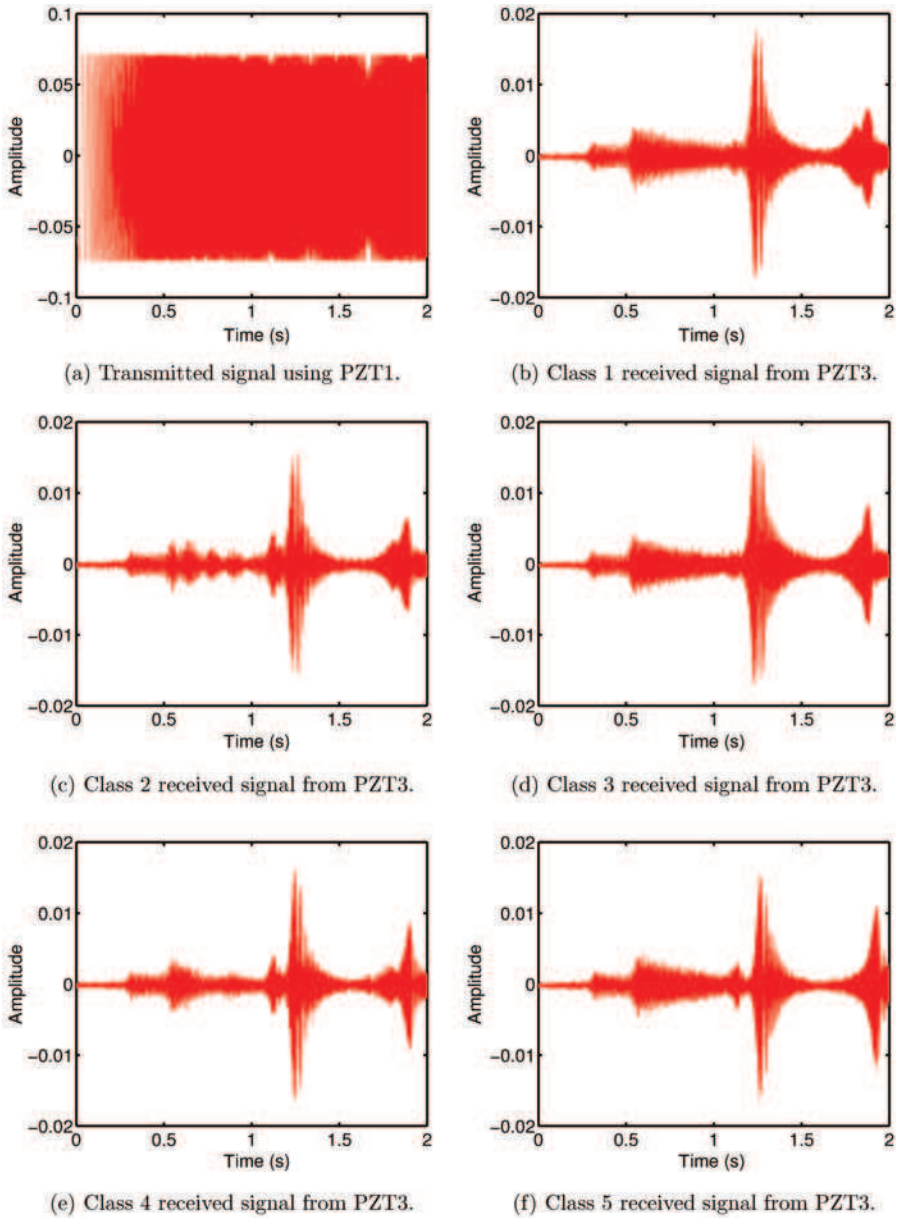

(a) Transmitted signal using PZT1.
(b) Class 1 received signal from PZT3.
(c) Class 2 received signal from PZT3.
(d) Class 3 received signal from PZT3.
(e) Class 4 received signal from PZT3.
(f) Class 5 received signal from PZT3.

Figure 7. *Example time-domain plots showing the signal transmitted by PZT1 and the signals received by PZT3 for the five different classes.*

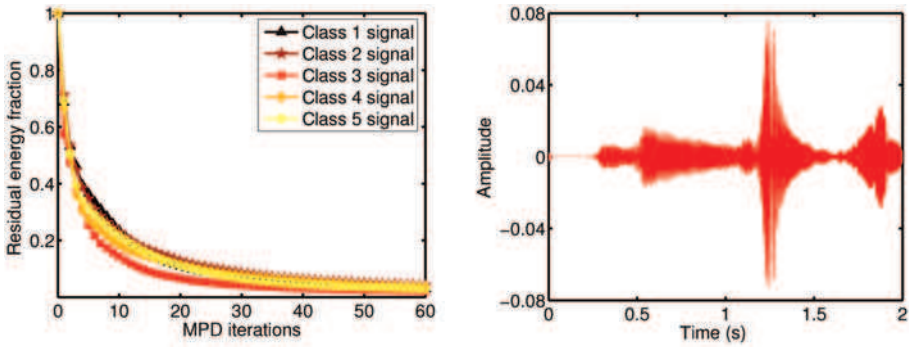

(a) Residue energy versus MPD iteration number.
(b) Class 1 signal from PZT3.

Figure 8. *(a) Residue energy vs. MPD iteration number. (b) Time-domain PZT3 Class 1 signal after preprocessing and after it decomposition using the MPD with N = 60 iterations. This is the processed version of the signal in Figure 7(b).*

$N = 60$ MPD iterations. Figure 8 shows the energy of the residue at each MPD iteration. The residue energy decreases at each successive iteration and reaches about 5% of the original signal energy in 60 iterations.

The MPD-TFRs of signals in Figure 7(b)–(f) are shown in Figures 9(b)–(f). It can be seen that the locations of the atoms with high energy correspond to positions of high amplitude in the signals in Figures 7(b)–(f).

Performing MPD with a dictionary of 42 million atoms for 10,800 signals, each of which was 10,000 samples long, is a challenging task. In order to reduce computational time, C programming language was used and the algorithm was implemented in parallel on a computing cluster using Message Passing Interface (MPI). The cluster consisted of seven 3 GHz dual-core Intel Pentium D processors running on 32 bit LINUX (with 1 GB RAM per core). The parallelization efficiency of the MPD implementation is shown in Figure 10. The run-time can be modeled as a function of the number of processors using the model $c_1 + c_2(N_w/N_p)$, where c_1 is the pre-computation cost common to all processors, c_2 is the computational cost (per signal) of the parallelizable part of the code, N_w is the total number of signals, and N_p is the number of

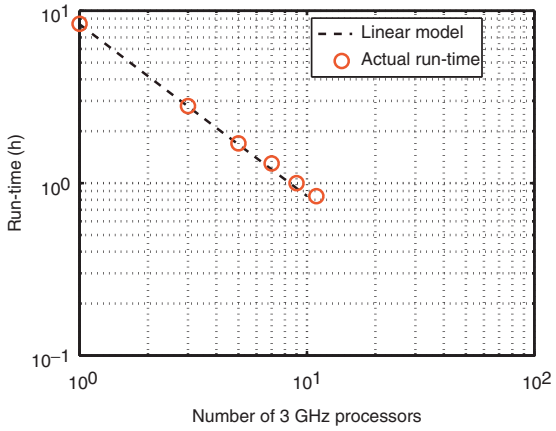

Figure 10. *Parallelization efficiency of the MPD implementation.*

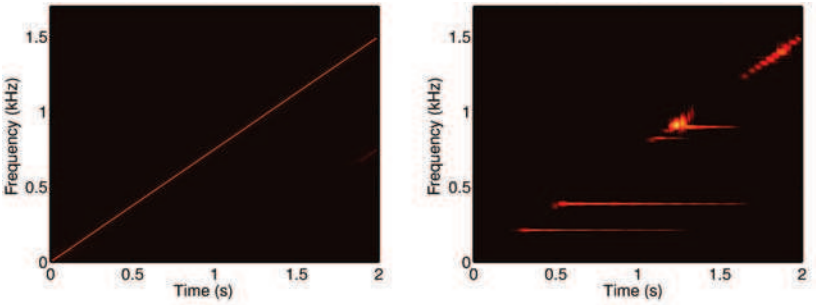

(a) WD of the transmitted signal using PZT1. (b) MPD-TFR of Class 1 signal from PZT3.

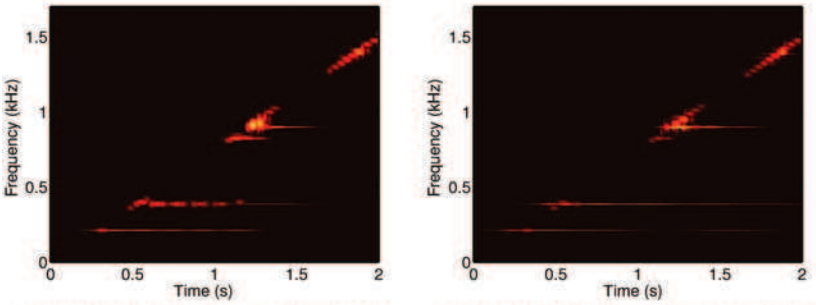

(c) MPD-TFR of Class 2 signal from PZT3. (d) MPD-TFR of Class 3 signal from PZT3.

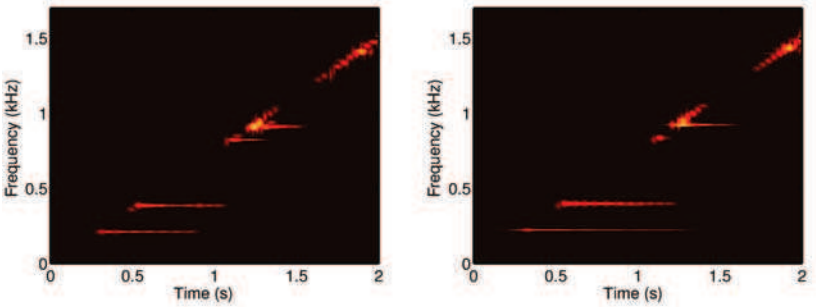

(e) MPD-TFR of Class 4 signal from PZT3. (f) MPD-TFR of Class 5 signal from PZT3.

Figure 9. *Example time-frequency plots showing: (a) WD (magnitude) of the transmitted signal, and (b)–(f) the MPD-TFRs of the PZT3 signals from the five classes after preprocessing and N = 60 MPD iterations.*

processing cores. The small discrepancy between the actual run-times and those predicted by the model is due to the fact that this model does not account for communication costs and possible network delays.

Optimizing the MPD-TFR Classifier

When physics-based models on structural damage are incorporated into the damage analysis and classification algorithms, the resulting performance can improve. This is demonstrated next, where prior knowledge using finite element analysis helps to improve the MPD classification performance.

Specifically, the MPD feature vectors from the various damage classes were observed to have a potential problem. The first few atoms extracted by the MPD have similar time-frequency shift and scale parameters, regardless of the actual signal classification. Since the first few MPD extracted atoms are also the highest in energy, they are the strongest contributors to the correlations used for classification. This is a problem as the classification is then effectively based on features that convey little or no discriminatory information. This is demonstrated in Figure 11 by superimposing the power spectral density (PSD) plots of multiple signals (from different damage classes) collected from the PZT3 sensor (solid lines) and the PSD plot of the MPD representation of one of the signals with only $N=3$ extracted atoms (dotted line). As it can be seen, the peaks lie in the same spectral regions, showing that there is significant frequency content overlap between signals from different damage classes. Similar analysis of data from PZT2 and PZT4 sensors, which are geometrically positioned further from the actuator than the PZT3 sensor as shown in Figure 6, indicates that the first 6 – 7 atoms in the MPD representation are similar for signals from all five classes.

In trying to explain this phenomenon, finite element analysis (FEA) is conducted to study the effects of damage on material properties and wave propagation. This analysis, provided in Appendix 7, demonstrates that the common frequencies correspond to the resonant frequencies of the plate, which lie in the excitation range 0–1.5 kHz. Since the resonant frequencies affect signals from different classes in a similar way, the MPD analysis and classification benefits from simply disregarding the first few high-energy MPD extracted atoms.

The identification of the MPD atoms that need to be discarded before classification can be carried out using cross-validation. This method finds the best combination of atoms to be discarded by validating the performance of the classifier on a separate data set, known as the validation set. However, this technique requires additional experimental data to form the validation set and can be expensive when the number of possible combinations of atoms is large. Instead of doing cross-validation, the finite element modeling can be used to determine the excitation resonant frequencies of the structure under investigation. These frequencies can then be compared with the parameters of the extracted MPD atoms in order to determine, which ones are common to all the classes. While finite element modeling and simulation of complex structural systems can be difficult, the method provides a reliable way of removing the redundant atoms. Details of the 3D finite element modeling analysis of the aluminum plate are given in Appendix.

MMPD and Dictionary Size

As discussed in section 'Modified MPD classifier', the MMPD is a parsimonious decomposition as it uses real signals to form the dictionary. In this application, only $N=2$ MMPD iterations were needed to reduce the residue energy to 5–10% of the signal energy. This is demonstrated in Figure 12 that shows the fast convergence of the MMPD. As the dictionary is composed of time-frequency shifted versions of the real data, the signals to be decomposed are well-matched

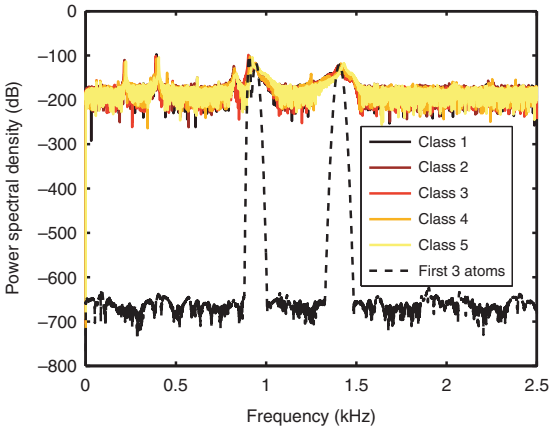

Figure 11. *Superimposed PSD of multiple PZT3 signals from each of the five classes and of one PZT3 MPD represented signal after $N=3$ iterations.*

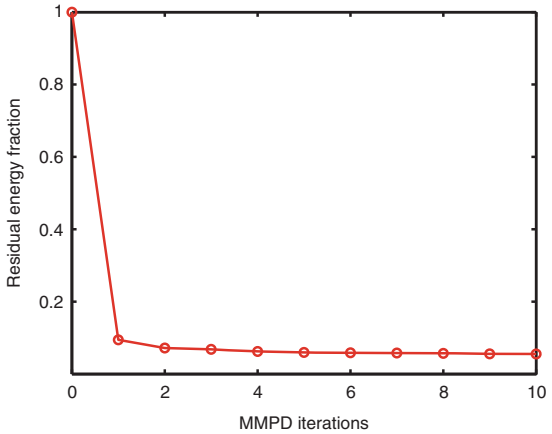

Figure 12. *Residue energy fraction vs. MMPD iterations.*

to the dictionary. Also, the time-frequency area of interest is more localized as it depends on the time-frequency content of the data. For example, frequency shifts from 0 to 25 Hz, in steps of 0.25 Hz, were found to be sufficient for this dictionary. For Gaussian dictionary MPDs, 42 million atoms were required in the dictionary in order to reduce the residue energy; for the real data dictionary MPD, similar energy reduction results were obtained with only 6 million dictionary atoms. The computational overhead due to lack of closed form expressions for the atoms was more than offset by the benefits of a smaller dictionary. In addition, the far fewer MMPD iterations needed to decompose the signal accurately also added to the computational advantage of the MMPD over the MPD.

Classification Results

The data recorded by the PZT sensors was divided into three sets. The first set was used for training, the second set was used for cross-validation, and the third set was used for testing. The signals from PZT2, PZT3, and and PZT4 were represented using $N = 60$ MPD iterations, corresponding to an average energy residue of about 5%. In the MPD-TFR-based damage classifier, the first 6, 3, and 7 MPD atoms were discarded from signals from PZT2, PZT3, and PZT4, respectively (section 'Optimizing the MPD-TFR Classifier').

The performance of the algorithm is demonstrated using a confusion matrix, as shown on Table 1 Panel (A) for PZT2 data classification. The confusion matrix element $C_{i,j}$, ith row and jth column, estimates the probability that a signal actually from damage Class i is classified as belonging to damage Class j. Here, i and j correspond to the five classes of fastener damage defined earlier. For example, in Table 1 Panel (A), $C_{5,5} = 0.98$ because 98% of the signals from Class 5 were (correctly) classified to Class 5. Note that the entries in each row of a confusion matrix add up to unity. The mean $1/M \sum_{i=1}^{M} C_{i,i}$ of the diagonal elements in the confusion matrix can be used as a measure of the average correct classification rate, where M is the total number of classes.

Table 1 shows the confusion matrices for MPD-TFR-based damage classification performed using data from PZT2, PZT3, and PZT4, without disregarding any atoms from the MPD decomposition. The average correct classification rates observed for data from PZT2, PZT3, and PZT4 are 78.4, 60, and 59.8%, respectively. The classification performance is thus poor, as explained by the finite element modeling analysis conducted on the test sample. Specifically, the principal modal frequencies are not altered by the induced damage, and the most dominant MPD atoms are common to all the classes. When those atoms are discarded, the classification performance improves significantly, as shown in Table 2. The average correct classification rates observed for data from PZT2, PZT3, and PZT4 are 87.6, 94, and 93.2%, respectively.

In order to demonstrate the improvement afforded by the time-frequency analysis, the classification results obtained from the MPD-TFR algorithm are compared with those from a baseline time-domain method. In this method, classification is performed directly using time-domain correlations. A representative template signal is computed for each damage class by averaging the training signals available from that class. A testing signal is classified by maximizing the time-domain correlation value of the testing signal with the template signals for each damage class.

Table 1. MPD classification results without optimization.

Class	1	2	3	4	5
Panel (A): MPD classification results for data from PZT2					
1	**0.94**	0.00	0.06	0.00	0.00
2	0.58	**0.00**	0.38	0.04	0.00
3	0.00	0.00	**1.00**	0.00	0.00
4	0.00	0.00	0.00	**1.00**	0.00
5	0.00	0.00	0.00	0.02	**0.98**
Panel (B): MPD classification results for data from PZT3					
1	**0.00**	0.00	0.38	0.62	0.00
2	0.00	**0.00**	0.13	0.87	0.00
3	0.00	0.00	**1.00**	0.00	0.00
4	0.00	0.00	0.00	**1.00**	0.00
5	0.00	0.00	0.00	0.00	**1.00**
Panel (C): MPD classification results for data from PZT4					
1	**1.00**	0.00	0.00	0.00	0.00
2	0.96	**0.00**	0.00	0.04	0.00
3	1.00	0.00	**0.00**	0.00	0.00
4	0.00	0.00	0.00	**1.00**	0.00
5	0.00	0.00	0.00	0.01	**0.99**

Table 2. MPD classification results with optimization.

Class	1	2	3	4	5
Panel (A): MPD classification results for data from PZT2					
1	**0.89**	0.11	0.00	0.00	0.00
2	0.10	**0.87**	0.00	0.03	0.00
3	0.00	0.38	**0.62**	0.00	0.00
4	0.00	0.00	0.00	**1.00**	0.00
5	0.00	0.00	0.00	0.00	**1.00**
Panel (B): MPD classification results for data from PZT3					
1	**0.77**	0.00	0.23	0.00	0.00
2	0.01	**0.96**	0.00	0.03	0.00
3	0.00	0.00	**1.00**	0.00	0.00
4	0.00	0.02	0.00	**0.97**	0.01
5	0.00	0.00	0.00	0.00	**1.00**
Panel (C): MPD classification results for data from PZT4					
1	**0.82**	0.09	0.06	0.03	0.00
2	0.03	**0.94**	0.00	0.03	0.00
3	0.00	0.09	**0.91**	0.00	0.00
4	0.01	0.00	0.00	**0.99**	0.00
5	0.00	0.00	0.00	0.00	**1.00**

The time-domain correlation based damage classifier was tested on data from PZT4 and the results are shown in the confusion matrix shown in Table 3. While the correct classification rates are good for classes 1, 3, 4, and 5, Class 2 signals are completely misclassified. The average correct classification rate is 77.2%. This is in contrast to the MPD-TFR classification results on the same PZT4 data (Table 2 Panel (C)), where the average correct classification rate is 93.2%. This illustrates the unreliability of the time-domain classifier, and confirms the robustness advantage offered by the MPD-TFR damage classifier.

When the MMPD-based damage classifier is used for classification, training signals from all classes are used to create the MMPD dictionary. As a result, there is no one atom that is common to all the classes of damage. Misclassification occurs in this method only if the time-frequency signature of the signals from one class is very similar to that of another class. Table 4 shows the classification results for the MMPD algorithm, using data from PZT3. The average correct classification rate is 98.8%, where the corresponding rate using the MPD-TFR classifier with PZT3 signals is 94%. In addition, the MMPD used a dictionary consisting of 6 million atoms as opposed to the 42 million atom dictionary used for the MPD-TFR classifier. The MMPD also needed only 1 or 2 iterations to achieve a residue energy of about 5% of the original signal whereas 60 iterations were used by the MPD-TFR classifier. Note, however, that the MMPD dictionary is very application specific and is limited by the acquired training data. Also, there is no analytic form of the dictionary components, and this may add to the processing time. Nevertheless, due to the smaller dictionary size and reduced number of required iterations, the computation time of the MMPD classification was less than that of the MPD-TFR-based classification.

Table 3. Time-domain correlation based classification results for data from PZT4.

Class	1	2	3	4	5
1	**0.96**	0.00	0.02	0.02	0.00
2	0.51	**0.00**	0.46	0.03	0.00
3	0.08	0.00	**0.91**	0.01	0.00
4	0.00	0.00	0.01	**0.99**	0.00
5	0.00	0.00	0.00	0.00	**1.00**

Table 4. MPD classification results for data from PZT3.

Class	1	2	3	4	5
1	**0.94**	0.00	0.06	0.00	0.00
2	0.00	**1.00**	0.00	0.00	0.00
3	0.00	0.00	**1.00**	0.00	0.00
4	0.00	0.00	0.00	**1.00**	0.00
5	0.00	0.00	0.00	0.00	**1.00**

BAYESIAN SENSOR FUSION

In SHM, data is often available from multiple sensors located at different physical positions. The goal of sensor fusion is to combine the information received from multiple sensing devices in a coherent manner so as to increase the overall damage detection performance.

If $x^{(k)}(t)$, $k = 1, \ldots, K$, is the data from the kth sensor, then an optimal Bayesian data fusion scheme relies on the *joint* density function, $p(x^{(1)}(t), \ldots, x^{(K)}(t)|C_m)$, of the data under class assumption C_m. Specifically, the data is assigned to class m^* if

$$m^* = \underset{m=1,\ldots,M}{\operatorname{argmax}} \left\{ p(x^{(1)}(t), \ldots, x^{(K)}(t) \middle| C_m) \right\},$$

where a uniform prior density $p(C_m)$ is assumed for simplicity. As the joint density is often difficult to model, the marginals $p(x^{(k)}(t)|C_m)$, $k = 1 \ldots, K$, can be used for the classification. Thus, the data from sensor k is assigned to class m^* if

$$m^* = \underset{m=1,\ldots,M}{\operatorname{argmax}} \left\{ p(x^{(k)(t)} \middle| C_m) \right\}.$$

The sensor data fusion problem is now transformed (sub-optimally) into a decision fusion problem, where the local decisions at each sensor are combined. Defining the discrete indicator variables $l^{(k)} = j$ if the data at the kth sensor is classified to Class j, the joint density function of the local decisions $p(l^{(1)} \ldots, l^{(K)}|C_m)$ is used in the Bayesian decision fusion to assign the data to Class m^* if

$$m^* = \underset{m=1,\ldots,M}{\operatorname{argmax}} \left\{ p(l^{(1)}, \ldots, l^{(K)} \middle| C_m) \right\}. \tag{5.1}$$

In practice, it is often convenient to assume statistical independence of the local decisions, so that $p(l^{(1)} \ldots, l^{(K)}|C_m) = \prod_{k=1}^{K} p(l^{(k)}|C_m)$ in (5.1). The marginal density functions $p(l^{(k)}|C_m)$, $k = 1 \ldots, K$, can generally be estimated more reliably than the full joint density, and are available directly from the local confusion matrices as $p(l^{(k)} = j|C_m) = C^k_{m,j}$, where $C^k_{m,j}$ is the mth row and jth column element of the confusion matrix at sensor k. Note that this Bayesian decision fusion approach can also be used to integrate information flow from multiple sensing modalities and even multiple local detection algorithms. This kind of fusion is especially advantageous in situations where some sensors and algorithms might be in a better position to classify damage from certain classes than others. A schematic of the sensor fusion scheme used here is shown in Figure 13.

The average correct classification rates obtained from the MPD-TFR classifier are based on using data from individual sensors only. When the sensor fusion algorithm is used with the MPD-TFR classifier to combine the information received from all the sensors, then the corresponding results are shown in Table 5. As it can be seen, the overall performance of the system improved significantly as the average correct classification rate with sensor fusion is 97.4%, as compared to 87.6, 94, and 93.2% when PZT2 sensor, PZT3 sensor, and PZT4 sensor were used alone, respectively (sensor fusion was not applied with the MMPD classifier because the classification performance using data from individual sensors was already very good).

CONCLUSIONS

The article develops a time-frequency-based damage classification technique. The method is based on decomposing signals using the MPD algorithm and then utilizing joint time-frequency analysis to discriminate between data from various damage conditions. Two different dictionaries are considered for the decomposition. The first dictionary consists of time-frequency shifted and scaled versions of a basic Gaussian atom; the second dictionary uses time-frequency shifted versions of real measured data from sensors (modified MPD or MMPD). The MPD-TFR classifier uses training and validation data sets to compute representative MPD-TFRs for each damage class and to validate model parameters. Classification of test data is performed based on the strength of 2D time-frequency correlations between MPD-TFRs of training data and the MPD-TFR of the test signals. The MMPD classifier uses training data to build the dictionary, and signals are classified according to the magnitude of the projections onto the various damage classes. A Bayesian sensor (decision) fusion approach is described to help improve classification performance by combining the information collected by multiple distributed sensors.

When applied to the detection of fastener failure damage in an aluminum plate, the MPD-TFR classifier yields an average correct classification rate of 91.6% and the MMPD classifier yields an average correct classification rate of 98.8%. The MMPD classifier yields more accurate classification results than the MPD-TFR classifier, while remaining computationally efficient as it uses a smaller dictionary and requires fewer MPD iterations. The MPD TFR classifier has some analytical and computational advantages, due to the availability of closed-form expressions for the dictionary atoms. Importantly, the dictionary here is not limited by the acquired training data. However, the MPD-TFR-based classifier suffers from the ill-effect of dominant atoms common to the different damaged classes. These redundant atoms, however, can be identified using either cross-validation or finite element analysis, and removed to improve classification. The Bayesian decision fusion improved the average correct classification rate of the MPD-TFR classifier to 97.4%. The decision fusion procedure employed requires additional data and computational effort in order to learn the statistics of the local classifiers.

Note that the data required for training the classification algorithms need not be experimentally collected; it can be numerically simulated using finite element analysis. This is important because it allows for the direct integration of physics based modeling with signal processing. The idea is to make use of the data computed from physically based models to learn the parameters of the time-frequency damage classification algorithms. Since this approach does not require the slow and expensive collection of experimental data, it is expected to yield significant savings in design time, complexity, and costs. The damage classification

Table 5. MPD classification results with sensor fusion.

Class	1	2	3	4	5
1	**0.92**	0.00	0.08	0.00	0.00
2	0.01	**0.97**	0.00	0.02	0.00
3	0.01	0.00	**0.99**	0.00	0.00
4	0.00	0.01	0.00	**0.99**	0.00
5	0.00	0.00	0.00	0.00	**1.00**

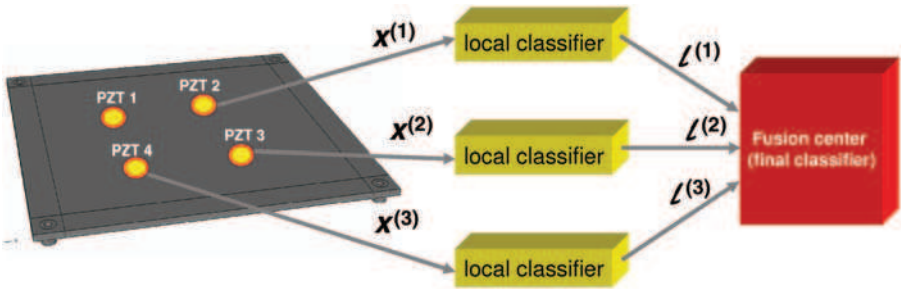

Figure 13. *Sensor fusion approach.*

technique presented in this article follows a general framework and has the advantage of being easily extended to many other related problems of interest such as damage detection, localization, or quantification. Note that training data is required to be available from each class of interest, and the training data needs to account for variability in the data due to environmental or operational conditions. Current work involves adapting the proposed algorithms to respond to various structural condition changes.

ACKNOWLEDGMENTS

The work was supported by the Department of Defense Air Force Office of Scientific Research Grant FA95550-06-1-0309 (Program manager: Dr Victor Giurgiutiu). Special thanks to M. Derriso, M. DeSimio, and S. Olson (AFRL, Wright Patterson AFB) for the experimental data, and to the reviewers for their comments that helped improve the document.

APPENDIX

3D Finite Element Modeling

In practical applications with irregular boundaries, finite element analysis (FEA) methods are used with the general purpose non-linear finite element software Abaqus (2007). The geometry of the aluminum plate and the holes and their locations (Figure A.1) that were modeled using 3D FEA are identical to those used in the experiments in (Olson et al., 2006). The boundary conditions of the plate bolted at the four corners are simulated such that each bolt is supported on a linear elastic spring along three coordinate axes with spring stiffness k_1, k_2, and k_3, respectively. The varying fastener torque affects the support stiffness from the bolts and nuts, and changing the spring stiffness affects the natural frequencies of the plate. To simulate the support stiffness, a connecting washer is inserted between the nuts and the plate. The stiffness of the washer is calibrated such that the first natural frequency from the simulation closely approximates the experimental result (Olson et al., 2006). Based on the assumption that the contact area between the nut and the washer is annular, the four supporting hexagonal nuts have been simulated as circular in shape. Hence, the plate is connected to the washers with the support stiffness, and the washers are connected to the nuts. The ends of the nuts are fixed as shown in Figure 1A(a).

Two cases are considered in the analysis. The first case involves the support stiffness of the washer being calibrated using the frequencies of all the four bolts at 100% torque. This was carried out by the authors of (Olson et al., 2006) using experimental modal analysis. In the second case, three bolts were considered at 100% torque and one bolt at 25% torque. The stiffness on the three bolts at 100% torque were chosen to be the same as before but the stiffness on the 25% torque was calibrated using the experimental modal analysis (EMA) results (Olson et al., 2006), as the correct stiffness of the bolt at this torque is not known. The FEA meshes are shown in Figure 1A(b). The center part of the plate was modeled as a 20-node quadratic brick with reduced integration elements ($C_3D_{20}R$) (Abaqus, 2007). A 10-node modified quadratic tetrahedron element ($C_3D_{10}M$) was used for the four corners, and a 4-node linear tetrahedron element (C_3D_4) was used for the nuts and washers. In total, 24,863 elements, 121,719 nodes, and 365,157 degrees of freedom were used in the modal analysis. There were two elements along the thickness of the plate, and the element length was about 3 mm.

During the calibration, a simple way to adjust the support stiffness was by altering the Young's modulus of the washer. The final material properties used in this study for the washers, plate, and nuts are listed in Table 1A. The simulated natural frequencies that lie within 1.5 kHz are listed in Tables 2A (all bolts at 100%) and 3A (one bolt at 25%). Note that the EMA results were not available for all the modes. Those entries in the tables are marked with a dashed line.

It can seen that the simulated results are in close agreement with the experimental ones. This is expected as FEA can simulate a structure with complex geometry

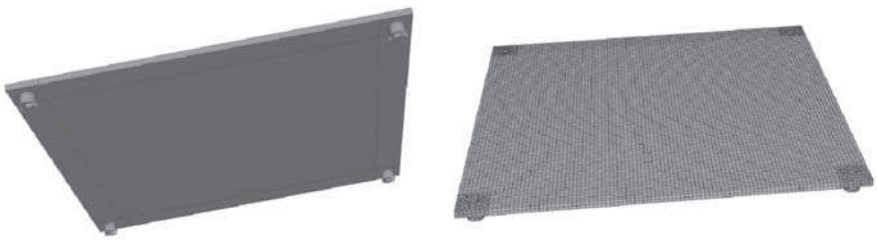

(a) Boundary condition connects and washers. (b) Meshes.

Figure 1A. *Boundary conditions and meshes for the aluminum plate.*

Table A1. Material properties used for washers, plate, and nuts.

	Young's modulus (E, GPa)	Poisson's ratio (ν)	Plate density (ρ, kg/m^3)
Aluminum	70	0.33	2870
Steel	200	0.32	7800
Washer at 100% torque	8	0.32	1000
Washer at 25% torque	2.5	0.32	1000

Table 2A. Modal frequencies with all bolts at 100% (dashed lines indicate data unavailable.

Mode	EMA (Hz)	FEA (Hz)	Difference (%)
1	185.05	185.1	0.02702
2	343.28	339.42	1.12445
3	–	339.6	–
4	388.78	382.53	1.60759
5	706.06	696.13	−1.4064
6	786.00	786.44	0.05598
7	843.37	853.7	1.224848
8	–	854.09	–
9	1119.75	1118.4	−0.12056
10	1263.84	1266.4	0.202557
11	–	1267.1	–
12	1591.14	1577.9	0.83211

Table 3A. Modal frequencies with one bolt at 25% torque and three bolts at 100% torque (dashed lines indicate data unavailable).

Mode	EMA (Hz)	FEA (Hz)	Difference (%)
1	181.25	181.30	0.027586
2	336.80	331.67	1.52316
3	–	335.86	–
4	384.76	377.36	1.92328
5	703.81	692.31	−1.63396
6	775.27	776.46	0.153495
7	831.46	840.96	1.142568
8	–	851.38	–
9	1106.58	1106.1	−0.04338
10	1254.98	1253.3	0.13387
11	–	1268.1	–
12	1580.07	1567.6	0.78921

and complex boundary conditions. In practice, there may be differences between the EMA and the numerical analysis. For example, in the EMA, there is an experimental measuring error that depends on the instrumental precision, simplifications in the FEA analyzed model, and boundary conditions. Nevertheless, good instrumentation and well-designed modeling can lead to good agreement of the results between EMA and FEA. The verified results confirm

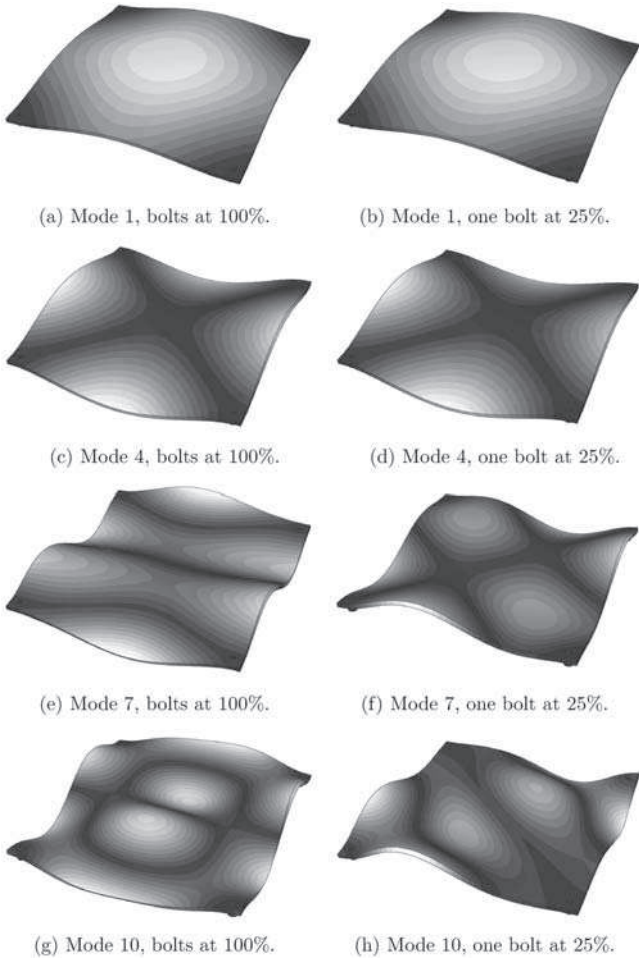

Figure 2A. *Example modes under different boundary conditions.*

that the model developed is accurate. Figure 2A shows the similarities and differences between the mode shapes in the material for four chosen modes with all bolts at 100% and one bolt at 25%. It is important to note that due to the symmetry of the plate, the amount of bolt looseness does not affect the mode shape of the plate. For example, modes 1 and 4 are similar (Figures 2A(a) and (d)). This implies that modal response-based damage detection techniques can lead to false conclusions.

REFERENCES

Abaqus 2007. Version 6.7.1.

Altes, R.A. April 1980. "Detection, Estimation and Classifcation with Spectrograms," *The Journal of the Acoustic Society of America*, 67(4):1232–1246.

Bernal, D. and Gunes, B. 2000. "An Examination of Instantaneous Frequency as a Damage Detection tool," In: *Engineering Mechanics Conference*, Austin, TX.

Chakraborty, D., Soni, S., Wei, J., Kovvali, N., Papandreou-Suppappola, A., Cochran, D. and Chattopadhyay, A. 2008. "Physics Based Modeling for Time-Frequency Damage Classification," In: *International Symposium on Smart*

Structures and Materials & Nondestructive Evaluation and Health Monitoring, Vol. 6926, San Diego.

Channels, L., Chakraborty, D., Simon, D., Kovvali, N., Spicer, J., Papandreou-Suppappola, A., Cochran, D., Peralta, P. and Chattopadhyay, A. 2008. ''Ultrasonic Sensing and Time-frequency Analysis for Detecting Plastic Deformation in an Aluminum Plate,'' In: *International Symposium on Smart Structures and Materials & Nondestructive Evaluation and Health Monitoring*, Vol. 6926, San Diego.

Cohen, L. 1994. *Time Frequency Analysis: Theory and Applications*, Prentice Hall.

Das, S., Papandreou-Suppappola, A., Zhou, X. and Chattopadhyay, A. 2005 ''On the use of the Matching Pursuit Decomposition Signal Processing Technique For Structural Health Monitoring,'' In: *SPIE International Symposium on Smart Structures and Materials*, Paper 5764-65, San Diego.

Das, S., Srivastava, A.N. and Chattopadhyay, A. 2007. ''Classification of Damage Signatures in Composite Plates Using One-class SVMs,'' In: *Aerospace Conference*, March 2007 IEEE, 1–19.

Doebling, S. and Farrar, C.R. 1998. ''Statistical Damage Identification Techniques Applied to the I-40 Bridge Over the Rio Grande,'' In: *International Modal Analysis Conference*, Santa Barbara, CA.

Ebenezer, S.P., Papandreou-Suppappola, A. and Suppappola, S.B. 2004. ''Classification of Acoustic Emissions Using Modified Matching Pursuit,'' *EURASIP Journal on Applied Signal Processing*, 3:347–357.

Eren, L. and Devaney, M.J. 2004. ''Bearing Damage Detection via Wavelet Packet Decomposition of the Stator Current,'' *IEEE Transactions on Instrumentation and Measurement*, 53:431–436.

Farrar, C., Nix, D., Duffey, T., Cornwell, P. and Pardoen, G. 1999. ''Damage Identification with Linear Discriminant Operators,'' In: *International Modal Analysis Conference*, Kissimmee, FL.

Farrar, C.R. and Lieven, N.A.J. 2007. ''Damage Prognosis: the Future of Structural Health Monitoring,'' *Royal Society of London Transactions Series A*, 365:623–632.

Farrar, C.R. and Worden, K. 2007. ''An Introduction to Structural Health Monitoring,'' *Philosophical Transactions of the Royal Society A*, 365:303–315.

Gelman, L., Giurgiutiu, V. and Petrunin, I. 2004. ''Advantage of Using the Fourier Components Pair Instead of Power Spectral Density for Fatigue Crack Diagnostics,'' *International Journal of Condition Monitoring and Diagnostic Engineering Management*, 7:18–22.

Hlawatsch, F. and Boudreaux-Bartels, G.F. 1992. ''Linear and Quadratic Time-frequency Signal Representations,'' *IEEE Signal Processing Magazine*, 9(2):21–67.

Jeong, H. and Jang, Y. 2000. ''Fracture Source Location in Thin Plates Using the Wavelet Transform of Dispersive Waves,'' *IEEE Transactions on Ultrasonics, Ferroelectrics, and Frequency Control*, 47:612–619.

Karasaridis, A., Maalej, M., Pantazopoulou, S. and Hatzinakos, D. 1997. ''Time-frequency Analysis of Sensor Data for Detection of Structural Damage in Instrumented Structures,'' In: *International Conference on Digital Signal Processing*, 2:817–820.

Mallat, S.G. and Zhang, Z. 1993. ''Matching Pursuits with Time-frequency Dictionaries,'' *IEEE Trans. on Signal Processing*, 41:3397–3415.

Mallat, S.G. July 1989. ''A Theory for Multiresolution Signal Decomposition: The Wavelet Representation,'' *IEEE Transactions on Pattern Analysis and Machine Intelligence*, 11(7):674–693.

Mallat, S. 1998. *A Wavelet Tour of Signal Processing*, 2nd edn. Academic Press.

Nguyen, M., Wang, X., Su, Z. and Ye, L., 2004. ''Damage Identifcation for Composite Structures with a Bayesian Network,'' In: *Intelligent Sensors, Sensor Networks and Information Processing Conference*, 307–311.

Olson, S.E., DeSimio, M. and Derriso, M.M. 2006. ''Fastener Damage Estimation in a Square Aluminum Plate,'' *Structural Health Monitoring*, 5:173–183.

Paget, C.A., Grondel, S., Levin, K. and Delebarre, C. 2003. ''Damage Assessment in Composites by Lamb Waves and Wavelet Coefficients,'' *Smart Materials and Structures*, 12(3):393–402.

Pakrashia, V., Basu, B. and Connora, A.O. 2007. ''Structural Damage Detection and Calibration Using a Wavelet-Kurtosis Technique,'' *Engineering Structures*, 29(9):2097–2108.

Papandreou-Suppappola, A. and Suppappola, S.B. 2002. ''Analysis and Classifcation of Timevarying Signals with Multiple Time-frequency Structures,'' *IEEE Signal Processing Letters*, 9:92–95.

Papandreou-Suppappola, A. (Ed.) 2002. *Applications in Time-Frequency Signal Processing*. CRC Press, Florida.

Park, G., Sohn, H., Farrar, C.R. and Inman, D.J. 2003. ''Overview of Piezoelectric Impedancebased Health Monitoring and the Path Forward,'' *Shock and Vibration Digest*, 35(6):451–463.

Sohn, H. and Farrar, C.R. June 2001. ''Damage Diagnosis using Time Series Analysis of Vibration Signals,'' *Smart Material Structures*, 10:446–451.

Sohn, H. and Law, K.H. 2000. ''Bayesian Probalistic Damage Detection of a Reinforced-concrete Bridge Column,'' *Earthquake Engineering Structural Dynamics*, 29:1139–1152.

Sohn, H., Farrar, C.R., Hunter, N.F. and Worden, K. 2001. ''Structural Health Monitoring Using Statistical Pattern Recognition Techniques,'' *Transactions of the ASME*, 123:706–711.

Sohn, H., Allen, D.W., Worden, K. and Farrar, C.R. 2005. ''Structural Damage Classification Using Extreme Value Statistics,'' *Journal of Dynamic Systems, Measurement, and Control*, 127:125–132.

Staszewski, W.J., Boller, C. and Tomlinson, G. 2004. *Structural Health Monitoring of Aerospace Structures, Smart Sensor Technologies and Signal Processing*. John Wiley and Sons, Ltd.

Sun, A. and Chang, C.C. July 2004. ''Statistical Wavelet-based Method For Structural Health Monitoring,'' *Journal of Structural Engineering*, 130(7):1055–1062.

Taha, M.M.R., Noureldin, A., Lucero, J.L. and Baca, T.J. 2006. ''Wavelet Transform for Structural Health Monitoring: A Compendium of Uses and Features,'' *Structural Health Monitoring*, 5(3):267–295.

Vincent, I., Doncarli, C. and Carpentier, E.L. 1994. ''Non Stationary Signals Classification Using Time-frequency Distributions,'' In: *IEEE-SP International Symposium on Time-Frequency and Time-Scale Analysis*, 233–236.